

Article

Phase Composition, Thermal Conductivity, and Toughness of TiO₂-Doped, Er₂O₃-Stabilized ZrO₂ for Thermal Barrier Coating Applications

Qi Wang¹, Lei Guo^{1,2,*}, Zheng Yan¹ and Fuxing Ye^{1,2}

¹ School of Materials Science and Engineering, Tianjin University, Tianjin 300072, China; mse_wangqi@tju.edu.cn (Q.W.); z_yan@tju.edu.cn (Z.Y.); yefx@tju.edu.cn (F.Y.)

² Tianjin Key Laboratory of Advanced Joining Technology, Key Lab of Advanced Ceramics and Machining Technology of Ministry of Education, Tianjin 300072, China

* Correspondence: glei028@tju.edu.cn; Tel.: +86-22-2740-6261

Received: 26 May 2018; Accepted: 17 July 2018; Published: 20 July 2018



Abstract: TiO₂ was doped into Er₂O₃-stabilized ZrO₂ (ErSZ) to obtain desirable properties for thermal barrier coating (TBC) applications. The phase composition, thermal conductivity, and mechanical properties of TiO₂-doped ErSZ were investigated. ErSZ had a non-transformable metastable tetragonal (*t'*) phase, the compound with 5 mol % TiO₂ consisted of *t'* and cubic (*c*) phases, while 10 mol % TiO₂ doped ErSZ had *t'*, *c*, and about 3.5 mol % monoclinic (*m*) phases. Higher TiO₂ doping contents caused more *m* phase, and the compounds were composed of *t'* and *m* phases. When the dopant content was below 10 mol %, TiO₂ doping could decrease the thermal conductivity and enhance the toughness of the compounds. At higher doping levels, the compounds exhibited an increased thermal conductivity and a reduction in the toughness, mainly attributable to the formation of the undesirable *m* phase. Hence, 10 mol % TiO₂-doped ErSZ could be a promising candidate for TBC applications.

Keywords: thermal barrier coatings; doping; phase stability; thermal conductivity; toughness

1. Introduction

Thermal barrier coatings (TBCs) exert an increasingly significant role as a surface protection technology in the field of modern gas turbines. They can enhance the resistance to high-temperature oxidation, corrosion, and erosion of the hot sections and provide thermal insulation, enhancing the inlet gas temperature, and improving the efficiency of the engines [1–3]. Up to now, the most widely used TBCs are made of 7–8 wt.% Y₂O₃-stabilized ZrO₂ (YSZ), due to its low thermal conductivity, good phase stability, large thermal expansion, and desirable fracture toughness [1–4]. The primary methods to produce TBCs are electron beam physical vapor deposition (EB-PVD), air plasma spraying (APS), and plasma spray physical vapor deposition (PS-PVD) [1,2,5–7].

YSZ TBCs are composed of a non-transformable metastable tetragonal (*t'*) phase that is stable below 1200 °C. At temperatures higher than 1200 °C, the *t'* phase becomes unstable, giving rise to a severe phase decomposition to cubic (*c*) and *t'* phases [2–4,8–10]. During cooling, the latter transforms to an *m* phase accompanied by a large volume expansion, severely damaging the TBCs. Additionally, YSZ undergoes accelerated sintering at high temperatures, leading to the TBCs with an increased thermal conductivity and a reduced strain compliance [2,11,12]. Demands for enhancing gas turbine efficiency have necessitated a significant increase in the combustion temperature. Hence, alternative TBC materials with even better phase stability, lower thermal conductivity, and higher toughness are strongly required.

Two main approaches have been developed to seek for novel TBC materials. One is exploring high-temperature ceramics with excellent phase stability and low thermal conductivity. These ceramics

include $Gd_2Zr_2O_7$, $GdPO_4$, $La_2Ce_2O_7$, doped CeO_2 , and $Y_3Al_5O_{12}$ [13–18]. However, by comprehensive investigations, these materials are found to have some undesirable properties, like poor fracture toughness and low thermal expansion coefficients, which affect their practical applications. The other is on the ZrO_2 -based systems with alternative stabilizers to Y_2O_3 [4,19–24]. Investigations have obtained remarkable success. It has been reported that, for rare earth oxides (RE_2O_3)-doped ZrO_2 , with the decrease of the RE^{3+} size, the phase stability of the t' phase increases, while the toughness decreases [4,13,19,20,24]. The rationale behind the phenomena might be related to the driving force for t' phase partitioning and the lattice tetragonality of the t' phase. Compared with YSZ, Yb_2O_3 -doped ZrO_2 is found to have high phase stability but low toughness [13,24]. Since the size of Er^{3+} is between those of Yb^{3+} and Y^{3+} , Er_2O_3 -doped ZrO_2 (ErSZ) may reveal better comprehensive properties, i.e., good phase stability and high toughness.

Low thermal conductivity is a primary criterion for selecting materials for TBC applications. Research indicates that doping TiO_2 into RE_2O_3 stabilized ZrO_2 can reduce the thermal conductivity, enhance the toughness, and improve the phase stability [25–28]. Therefore, this study is conducted on a ZrO_2 - Er_2O_3 - TiO_2 system, investigating the effects of TiO_2 doping on the phase composition, thermal conductivity, and toughness of the compounds. The compositions are ErSZ doped with x mol % TiO_2 ($x = 0, 5, 10, 15, 20$). The ErSZ powders are synthesized by a chemical co-precipitation method, and the pellets for property measurements are produced by a solid state reaction and sintering method.

2. Experimental Procedures

Er_2O_3 (purity 99.99%) and $ZrOCl_2 \cdot 8H_2O$ (purity 99.95%) were employed as raw materials to produce 3.5 mol % Er_2O_3 -doped Zirconia (ErSZ) powders by a chemical co-precipitation. Er_2O_3 powders and $ZrOCl_2 \cdot 8H_2O$ were dissolved in nitric acid and deionized water, respectively. The obtained solution was mixed according to the compositional requirement and stirred to generate a homogeneous solution, followed by adding it cautiously to excess ammonia water ($pH > 12$) until a gel-like precipitate was obtained. The precipitate was filtered with distilled water repeatedly and washed with alcohol until a neutral pH was acquired. After being dried at 120 °C for 10 h and calcinated at 800 °C for 5 h for crystallization, the resultant powders were ground and sieved to remove the coarse agglomerates.

TiO_2 doped ErSZ powders were synthesized by a solid state reaction method. First, the fabricated ErSZ powders were mixed with x mol % ($x = 0, 5, 10, 15, 20$) TiO_2 by ball milling (QM-3SP4, Nanjing University Instrument Factory, Nanjing, China) for 8 h. Afterward, the suspension liquid was dried at 150 °C for 12 h, followed by calcination at 1400 °C for 10 h. The obtained powders were cold pressed (NYL-2000D, Wuxi Jianyi Instrument & Machinery Co., Ltd., Wuxi, China) at ~250 MPa and sintered (SX-G05165, Tianjin Zhonghuan Experiment Electric Furnace Co., Ltd., Tianjin, China) at 1500 °C for 12 h to achieve pellets for thermal conductivity and toughness measurements.

The analysis of phase compositions was carried out by X-ray diffraction (XRD; D/MAX 2500, Rigaku Diffractometer, Tokyo, Japan) within a scanning range of $2\theta = 20^\circ$ – 80° . Additionally, for the sake of distinguishing the t' (t_1' , t_2') and c phases, slow scans were performed over the range of $2\theta = 72^\circ$ – 76° with a step size of 0.01° and a dwell time of 20 s.

Thermal diffusivity (α) was measured using a laser-flash apparatus (Netzsch LFA 427, Netzsch, Bavaria, Germany) from 20 to 1200 °C at an interval of 200 °C. Before the measurements, a thin graphite film was coated on the front and rear surfaces of the sample for thermal absorption of laser pulses. Each sample was measured three times at the concerned temperature. To obtain the thermal conductivity (λ), the following formula was employed:

$$\lambda = \rho \cdot \alpha \cdot C_p \quad (1)$$

where ρ is the density, which is measured by Archimedes method, and C_p is the specific heat capacity derived from the heat capacity values of the constituent oxides according to the Neumann-Kopp rule [29].

It was estimated that the uncertainty of the thermal conductivity was $\pm 5\%$, considering the uncertainties for the density, the thermal diffusivity, and the specific heat capacity. Since the bulk is porous, the actual data was obtained by correcting the measured thermal conductivity using the following equation [30]:

$$\frac{\lambda}{\lambda_0} = 1 - \frac{4}{3}\phi \quad (2)$$

where ϕ is the fractional porosity.

The mechanical properties of the pellet was measured by an indentation method. Although this method to determine the mechanical property of a material is uncertain, it could be used for qualitatively comparing a series of samples produced by similar procedures [13,24]. Hence, it was employed in this study to reveal the variation trend of the mechanical properties with the TiO_2 content. Vickers hardness (H_V) was measured on the polished surface of the samples with 3 kg load dwelling 15 s by an automatic turret digital Vivtorinox hardness tester (HV-1000A, Laizhou Huayin Testing Instrument Co., Ltd., Yantai, China). At least 15 valid indentations were taken for each sample. Fracture toughness (K_{IC}) was calculated from the radial crack pattern of Vickers indentations by the following equation [31].

$$K_{IC} = 0.16H_V a^2 c^{-3/2} \quad (3)$$

where a represents the half length of the indent diagonal, c is the half-crack length measured from the middle of the indent to the tip of the crack.

3. Results and Discussions

Figure 1 shows the XRD patterns of the ErSZ pellet and the compounds doped with different amounts of TiO_2 . In all the patterns, no diffraction peak ascribed to an Er_2O_3 or a TiO_2 phase could be detected, indicating that a ZrO_2 -based solid solution has been produced. All the compounds are mainly composed of t' phase. However, when the TiO_2 content reaches to 10 mol %, an m phase is formed. With the increase of the TiO_2 content, the m phase to t' phase peaks intensity ratio increases, suggesting that more m phase forms. Since many diffraction peaks of t' and c phases are often overlapped in the XRD patterns, it is difficult to preclude the c phase just according to Figure 1.

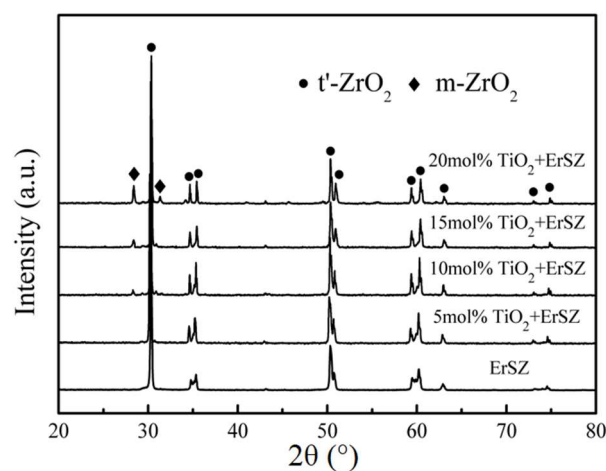


Figure 1. X-ray diffraction (XRD) patterns of the ErSZ pellet and the compounds doped with TiO_2 .

To further identify the phase constitution, $\{004\}$ diffraction peaks at $2\theta = 72^\circ\text{--}76^\circ$ were examined in detail by slow scans. As observed in Figure 2, ErSZ only consists of a t' phase, which decomposes

to t_1' and t_2' phases in other specimens. Here, t' , t_1' and t_2' phases all have a tetragonal structure, but with different dopant contents. In the XRD patterns of the compositions with 5 mol % and 10 mol % TiO_2 , a $(400)_c$ peak appears indicative of the formation of a c phase. Higher TiO_2 doping causes the disappearance of the c phase. Therefore, according to the XRD analysis, it could be concluded that ErSZ is composed of a t' phase, the compounds with 5 mol % consist of t' ($t_1' + t_2'$) and c phases, 10 mol % TiO_2 doping leads to the formation of t' ($t_1' + t_2'$), c and m phases. While at higher doping levels, the compounds have m and t' phases. The phase contents of the compounds are listed in Table 1. It could be found that 10 mol % TiO_2 doped ErSZ has the lowest m phase content, about 3.5 mol %.

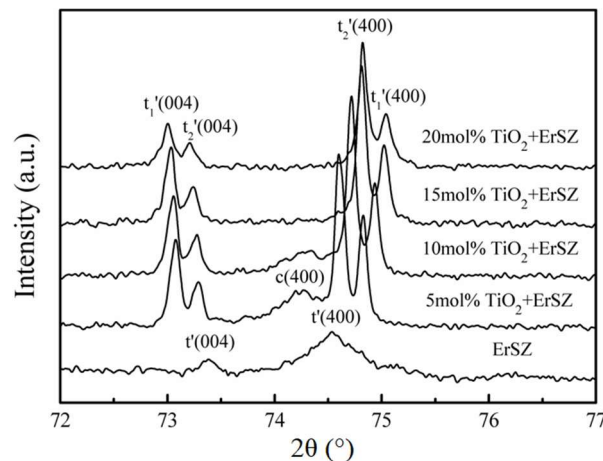


Figure 2. X-ray diffraction peaks of TiO_2 doped ErSZ at $2\theta = 72^\circ\text{--}76^\circ$ by slow scans.

Table 1. Phase compositions of 10 mol %, 15 mol %, and 20 mol % TiO_2 -doped ErSZ.

TiO_2 Content (mol %)	c	$t_1' + t_2'$	m
10	7.8	88.7	3.5
15	0	91.8	8.2
20	0	87.6	12.4

Previous research has demonstrated that, in the $\text{TiO}_2\text{-Yb}_2\text{O}_3\text{-ZrO}_2$ solid solution, Ti^{4+} first occupies the interstitial sites when the content is ≤ 2.5 mol %, followed by substituting for Zr^{4+} at higher doping contents [28]. In TiO_2 -doped YbSZ series, YbSZ consists of a t' phase, small amounts of TiO_2 doping causes a c phase, and higher TiO_2 doping decreases the c phase content and produces an m phase. The solid-solution mechanism provides a reasonable explanation for the phase structure evolution of the TiO_2 doped compounds. In this study, the smallest doping content is 5 mol %, larger than the critical value for creating interstitial ions. Therefore, the evidence for the presence of interstitial ions cannot be observed through the XRD analysis. However, the phase evolution of TiO_2 -doped ErSZ can be explained by the solid-solution mechanism proposed in [28]. The formation of the c phase is due to the decreased average coordination numbers of cations caused by the presence of Ti^{4+} interstitial ions. Since Ti^{4+} ions are not evenly distributed in the solid solution, c and t' phases are both present in the compounds. At higher doping levels, the substitution of Ti^{4+} ion for Zr^{4+} generates overcrowding problems of O^{2-} ions, giving rise to a strain field in the lattice. Thus, the c and t' phases become unstable, producing an m phase.

Figure 3 shows thermal diffusivities of different amounts of TiO_2 -doped ErSZ in a temperature range of 20–1200 °C. Error bars are omitted due to their small size. The thermal diffusivity decreases with the temperature. At a selected temperature, the thermal diffusivity does not decrease monotonically with the TiO_2 content. Instead, it declines, followed by a growing tendency with increasing the TiO_2 content. The calculated thermal conductivity is shown in Figure 4. For each sample,

the thermal conductivity first decreases with the temperature, and then rises when the temperature is above 1000 °C. There is a strong correlation between the thermal conductivity and the TiO₂ content. TiO₂ doping initially decreases the thermal conductivity, while at higher doping levels, the samples reveal an increased thermal conductivity. In TiO₂-doped ErSZ series, the composition with 10 mol % TiO₂ has the lowest thermal conductivity, with a value of 1.71 W/mK at 1200 °C.

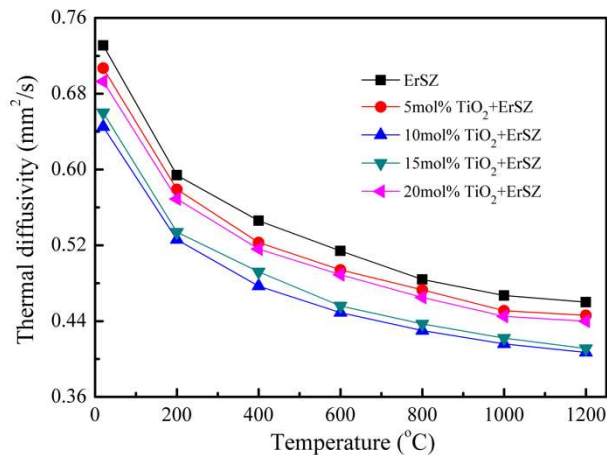


Figure 3. Thermal diffusivities of different amounts of TiO₂-doped ErSZ.

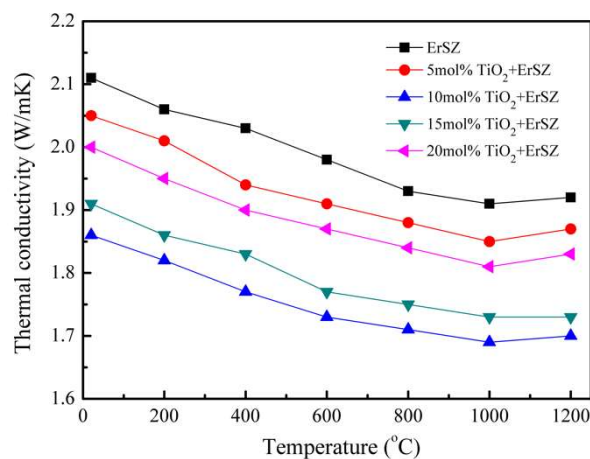


Figure 4. Thermal conductivities of different amounts of TiO₂-doped ErSZ.

Given the thermal conductivity theory in an electrical insulating substance, thermal conduction mainly depends on the phonons scattering. The stronger the phonon scattering, the shorter the phonon mean free path. A decline in the phonon mean free path leads to decreased thermal conductivity. The phonon mean free path is comprised of two parts, which can be expressed as follows [32,33]:

$$\frac{1}{l(\omega, T)} = \frac{1}{l_i(\omega, T)} + \frac{1}{l_p(\omega, T)} \quad (4)$$

where $l(\omega, T)$ is the phonon mean free path, $l_i(\omega, T)$ and $l_p(\omega, T)$ are the specific phonon mean free path due to the phonon-phonon scattering and the defect scattering, respectively, and ω and T refer to frequency and the corresponding temperature.

The ability of phonon scattering has a relationship with the phonon scattering coefficient (Γ), which is determined by the difference of atomic mass (Γ_M) and that of the ionic radius (Γ_δ). Considering

the effect of the anharmonicity in a solid solution expressed by an influence factor ϵ , the relation of Γ , Γ_M , and Γ_δ can be expressed in the following equations [27,33,34]:

$$\Gamma = \Gamma_M + \epsilon\Gamma_\delta \quad (5)$$

$$\Gamma_M = \frac{\sum f_i (M_i - \bar{M})^2}{(\bar{M})^2} \quad (6)$$

$$\Gamma_\delta = \frac{\sum f_i (\delta_i - \bar{\delta})^2}{(\bar{\delta})^2} \quad (7)$$

where M_i , δ_i , and f_i represent the atomic mass, the ionic radius, and the fractional content of the imperfection, respectively, \bar{M} and $\bar{\delta}$ are the average atomic mass and mean ionic radius of a specific site in the lattice, respectively.

Zr^{4+} , Er^{3+} , and Ti^{4+} have Shannon effective ionic radius of 0.84 Å, 1.004 Å, and 0.74 Å, respectively [35]. The substitution of Ti^{4+} for Zr^{4+} could cause elastic field in the ZrO_2 lattice. Additionally, due to the mass difference between Ti^{4+} and Zr^{4+} , mass fluctuation can also be introduced in the lattice. As a result, a large phonon scattering coefficient is obtained in the compounds, giving rise to stronger phonon scattering ability and a lower phonon mean free path [27,28,36]. Hence, the thermal conductivity of TiO_2 -doped ErSZ decreases with the increase of the TiO_2 content. At high doping levels (>10 mol % TiO_2), the compounds have an increased thermal conductivity, resulting from the m phase formation. Since the m phase has higher thermal conductivity than those of c and t' phases [2,20,21,37,38], it is reasonable to observe increased thermal conductivities for ErSZ doped with high TiO_2 contents.

The relative densities of the samples for mechanical measurements are above 95%. Vicker hardness (H_v) and toughness of the samples are both presented in Figure 5. It is possible to observe that TiO_2 -doped ErSZ reveals a nearly composition independent hardness. However, the toughness is sensitive to the composition. Increasing the TiO_2 doping content, the toughness of TiO_2 doped ErSZ first exhibits an upward variation trend, and then decreases when the doping content is above 10 mol %. Specially, 10 mol % TiO_2 doped ErSZ has the highest toughness, with a value of $\sim 6.09 \text{ MPa}\cdot\text{m}^{1/2}$, nearly 35% and 30% higher than that of ErSZ and YSZ, respectively [13].

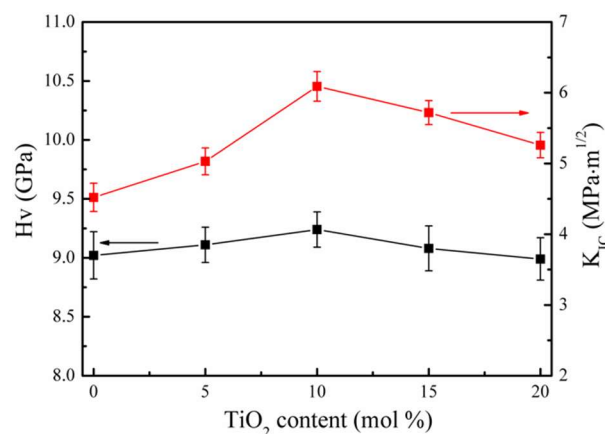


Figure 5. Vickers hardness and toughness of TiO_2 -doped ErSZ.

For a ZrO_2 -based ceramic consisting of t' , c , and m phases, the toughness could be considered as the weighted average of each phase [39]. Therefore, a qualitative comparison among the toughness values of TiO_2 -doped ErSZ can be made. ErSZ and the compositions with 5 mol % and 10 mol % TiO_2 contents are mainly composed of t' , while higher TiO_2 doping contents lead to the formation of an m

phase. Since the t' phase has higher toughness than that of the m phase [2,8,11,24], it is reasonable to obtain lower toughness when the doping content is at high levels.

As can be seen in Figures 1 and 2, 5 mol % TiO_2 -doped ErSZ is composed of t' and c phases, while ErSZ only has a t' phase. Since the c phase has a lower toughness than the t' phase, the 5 mol % TiO_2 -doped ErSZ should have lower toughness compared with ErSZ based on the aforementioned qualitative comparison, which is inconsistent with the result in Figure 5. Hence, another mechanism may contribute to the variation of the toughness. It is known that the high toughness of the t' phase is due to the ferroelastic toughening. Based on the mechanism, the ferroelastic domain existing in the compounds would switch around the crack tip when a high stress is applied, which absorbs the energy and thus induces the toughening effect. The increased fracture energy due to domain switching can be expressed as follow [39–41]:

$$\Delta\Gamma = 2fh\tau_c\gamma \quad (8)$$

where h represents the width of the domain switching process zone, f is the volume fraction of the domain that undergoes switching, τ_c is the coercive stress required for switching, and γ is the related ferroelastic strain, which is determined by the lattice tetragonality [39–41].

$$\gamma = \frac{2}{3}\left(\frac{c}{a} - 1\right) \quad (9)$$

where c and a are lattice constants of the t phase and c/a is the tetragonality. Assuming that the f and h values are identical for a series of compounds, the fracture energy increases with the increase of the lattice tetragonality.

Figure 6 shows the tetragonality of the t' phase (t_1' and t_2') in TiO_2 doped ErSZ. The value increases with the increase of the TiO_2 content. As a result, the ferroelastic strain increases, causing higher fracture energy and thus better toughness if only lattice variation is considered. Taking into consideration the effects of the tetragonality and the amount of the t' phase, the higher toughness of 5 mol % TiO_2 -doped ErSZ compared with ErSZ suggests that the tetragonality of the t' phase play a major role in affecting the toughness. However, the toughness increase rate from ErSZ to 5 mol % TiO_2 -doped ErSZ is slower than that from 5 mol % TiO_2 -doped ErSZ to the composition with 10 mol % TiO_2 , indicating that the effect of the c phase formation cannot be neglected. When the TiO_2 doping content is larger than 10%, although the tetragonality of t' phase still increases, the toughness shows a reduction trend, mainly attributable to the formation of the m phase and the obvious decrease in the t' phase amount. In this case, the t' phase content play a key role in affecting the toughness.

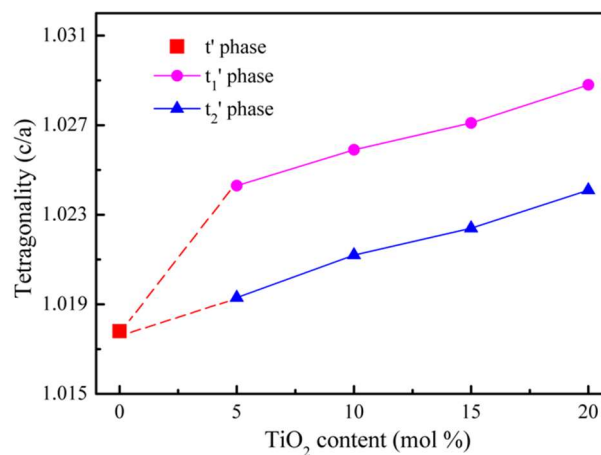


Figure 6. Tetragonality of the t' phase in TiO_2 -doped ErSZ.

TiO₂ doping has visible effects on the phase composition, thermal conductivity, and toughness of ErSZ. Among the compositions in the present study, it could be found that 10 mol % TiO₂-doped ErSZ reveals the lowest thermal conductivity and the highest toughness, which are desirable attributes for TBC applications. Based on this study, our future work will focus on producing 10 mol % TiO₂-doped ErbSZ TBCs to exploit advantages of this TBC candidate material to the full.

4. Conclusions

Compounds in a TiO₂-Er₂O₃-ZrO₂ system were fabricated, and their phase composition, thermal conductivity, and toughness were investigated. ErSZ exhibited a *t'* phase, 5 mol % TiO₂-doped ErSZ consisted of *t'* and *c* phases, whereas the composition with 10 mol % TiO₂ had had *t'*, *c*, and about 3.5 mol % *m* phases. At higher TiO₂ doping levels, the compounds are composed of *t'* and *m* phases. When the doping content is below 10 mol %, TiO₂ doping reduced the thermal conductivity and improved the toughness. The thermal conductivity and toughness of 10 mol % TiO₂-doped ErSZ were 1.71 W/mK (1200 °C) and ~6.09 MPa·m^{1/2}, respectively, obviously superior to those of ErSZ. However, higher TiO₂ doping contents had an adverse effect on the thermal conductivity and toughness of the compounds, which were attributed to the formation of the *m* phase. Given the low thermal conductivity and good toughness, 10 mol % TiO₂-doped ErSZ might be a promising TBC material.

Author Contributions: Conceptualization, L.G.; Methodology, Q.W. and Z.Y.; Validation, L.G. and F.Y.; Formal Analysis, Q.W. and L.G.; Investigation, Q.W. and Z.Y.; Data Curation, Q.W.; Writing-Original Draft Preparation, Q.W.; Writing-Review & Editing, L.G.; Supervision, L.G.

Funding: This research was funded by the National Natural Science Foundation of China (51501127 and 51375332) and the Natural Science Foundation of Tianjin (No. 16JCQNJC02900 and 16JCYBJC18700).

Acknowledgments: Great acknowledgement to Chenglong Zhang and Mingzhu Li, who provided much help.

Conflicts of Interest: The authors declare no conflict of interest.

References

1. Guo, H.; Vaßen, R.; Stöver, D. Atmospheric plasma sprayed thick thermal barrier coatings with high segmentation crack density. *Surf. Coat. Technol.* **2004**, *186*, 353–363. [[CrossRef](#)]
2. Vassen, R.; Jarligo, M.O.; Steinke, T.; Mack, D.E.; Stöver, D. Overview on advanced thermal barrier coatings. *Surf. Coat. Technol.* **2010**, *205*, 938–942. [[CrossRef](#)]
3. Padture, N.P. Advanced structural ceramics in aerospace propulsion. *Nat. Mater.* **2016**, *15*, 804–809. [[CrossRef](#)] [[PubMed](#)]
4. Wang, Y.; Zhou, C. Hot corrosion behavior of nanostructured Gd₂O₃ doped YSZ thermal barrier coating in presence of Na₂SO₄ + V₂O₅ molten salts. *Prog. Nat. Sci. Mater.* **2017**, *27*, 507–513. [[CrossRef](#)]
5. Msuer, G.; Du, L.; Vassen, R. Atmospheric plasma spraying of single phase lanthanum zirconate thermal barrier coatings with optimized porosity. *Coatings* **2016**, *6*, 49.
6. Zhang, W.; Li, G.; Zhang, Q.; Yang, G. Comprehensive damage evaluation of localized spallation of thermal barrier coatings. *J. Adv. Ceram.* **2017**, *6*, 230–239. [[CrossRef](#)]
7. Gao, L.; Wei, L.; Guo, H.; Xu, H. Deposition mechanisms of yttria-stabilized zirconia coatings during plasma spray physical vapor deposition. *Ceram. Int.* **2016**, *42*, 5530–5536. [[CrossRef](#)]
8. Tsipas, S.A. Effect of dopants on the phase stability of zirconia-based plasma sprayed thermal barrier coatings. *J. Eur. Ceram. Soc.* **2010**, *30*, 61–72. [[CrossRef](#)]
9. Renteria, A.F.; Saruhan, B. Effect of ageing on microstructure changes in EB-PVD manufactured standard PYSZ top coat of thermal barrier coatings. *J. Eur. Ceram. Soc.* **2006**, *26*, 2249–2255. [[CrossRef](#)]
10. Wang, Y.; Zhou, C. Microstructure and thermal properties of nanostructured gadolinia doped yttria-stabilized zirconia thermal barrier coatings produced by air plasma spraying. *Ceram. Int.* **2016**, *42*, 13047–13052. [[CrossRef](#)]
11. Clarke, D.R.; Phillpot, S.R. Thermal barrier coating materials. *Mater. Today* **2005**, *8*, 22–29. [[CrossRef](#)]
12. Liu, X.; Wang, X.; Javed, A.; Zhu, C.; Liang, G. The effect of sintering temperature on the microstructure and phase transformation in tetragonal YSZ and LZ/YSZ composites. *Ceram. Int.* **2016**, *42*, 2456–2465. [[CrossRef](#)]

13. Guo, L.; Li, M.; Zhang, C.; Huang, X.; Ye, F. Dy₂O₃ Stabilized ZrO₂ as a toughening agent for Gd₂Zr₂O₇ ceramic. *Mater. Lett.* **2017**, *188*, 142–144. [[CrossRef](#)]
14. Guo, L.; Li, M.; Zhang, Y.; Ye, F. Improved toughness and thermal expansion of non-stoichiometry Gd_{2-x}Zr_{2+x}O_{7+x/2} ceramics for thermal barrier coating application. *J. Mater. Sci. Technol.* **2016**, *32*, 28–33. [[CrossRef](#)]
15. Guo, L.; Li, M.; Cheng, Y.; Zhang, C.; He, S.; Zhang, Y.; Ye, F. Plasma sprayed nanostructured GdPO₄ thermal barrier coatings: Preparation microstructure and CMAS corrosion resistance. *J. Am. Ceram. Soc.* **2017**, *100*, 4209–4218. [[CrossRef](#)]
16. Wang, Y.; Guo, H.; Gong, S. Thermal shock resistance and mechanical properties of La₂Ce₂O₇ thermal barrier coatings with segmented structure. *Ceram. Int.* **2009**, *35*, 2639–2644. [[CrossRef](#)]
17. Chen, X.; Zhang, H.; Zhang, H.; Zhao, Y.; Li, G. Ce_{1-x}Sm_xO_{2-x/2}—A novel type of ceramic material for thermal barrier coatings. *J. Adv. Ceram.* **2016**, *5*, 244–252. [[CrossRef](#)]
18. Zhou, Y.; Lu, X.; Xiang, H.; Feng, Z. Preparation, mechanical, and thermal properties of a promising thermal barrier material: Y₄Al₂O₉. *J. Adv. Ceram.* **2015**, *4*, 94–102. [[CrossRef](#)]
19. Rebollo, N.R.; Fabrichnaya, O.; Levi, C.G. Phase stability of Y + Gd co-doped zirconia. *Zeitschrift für Metallkunde* **2003**, *94*, 163–170. [[CrossRef](#)]
20. Rahaman, M.N.; Gross, J.R.; Dutton, R.E.; Wang, H. Phase stability, sintering, and thermal conductivity of plasma-sprayed ZrO₂-Gd₂O₃ compositions for potential thermal barrier coating applications. *Acta Mater.* **2006**, *54*, 1615–1621. [[CrossRef](#)]
21. Feng, J.; Ren, X.; Wang, X.; Zhou, R.; Pan, W. Thermal conductivity of ytterbia-stabilized zirconia. *Scr. Mater.* **2012**, *66*, 41–44. [[CrossRef](#)]
22. Sun, L.; Guo, H.; Peng, H.; Gong, S.; Xu, H. Influence of partial substitution of Sc₂O₃ with Gd₂O₃ on the phase stability and thermal conductivity of Sc₂O₃-doped ZrO₂. *Ceram. Int.* **2013**, *39*, 3447–3451. [[CrossRef](#)]
23. Cairney, J.M.; Rebollo, N.R.; Rühle, M.; Levi, C.G. Phase stability of thermal barrier oxides: A comparative study of Y and Yb additions. *Int. J. Mater. Res.* **2007**, *98*, 1177–1187. [[CrossRef](#)]
24. Zhang, Y.; Guo, L.; Zhao, X.; Wang, C.; Ye, F. Toughening effect of Yb₂O₃ stabilized ZrO₂ doped in Gd₂Zr₂O₇ ceramic for thermal barrier coatings. *Mater. Sci. Eng. A Struct.* **2015**, *648*, 385–391. [[CrossRef](#)]
25. Schaedler, T.A.; Leckie, R.M.; Krämer, S.; Evans, A.G.; Levi, C.G. Toughening of nontransformable t'-YSZ by addition of titania. *J. Am. Ceram. Soc.* **2007**, *90*, 3896–3901. [[CrossRef](#)]
26. Chen, T.D.; Tekeli, S.; Dillona, R.P.; Mecartney, M.L. Phase stability, microstructural evolution and room temperature mechanical properties of TiO₂ doped 8 mol % Y₂O₃ stabilized ZrO₂ (8Y-CSZ). *Ceram. Int.* **2008**, *34*, 365–370. [[CrossRef](#)]
27. Zhao, M.; Pan, W. Effect of lattice defects on thermal conductivity of Ti-doped, Y₂O₃-stabilized ZrO₂. *Acta Mater.* **2013**, *61*, 5496–5503. [[CrossRef](#)]
28. Guo, L.; Zhang, C.; Xu, L.; Li, M.; Wang, Q.; Ye, F.; Dan, C.; Ji, V. Effects of TiO₂ doping on the defect chemistry and thermo-physical properties of Yb₂O₃ stabilized ZrO₂. *J. Eur. Ceram. Soc.* **2017**, *37*, 4163–4169. [[CrossRef](#)]
29. Kubaschewski, O.; Alcock, C.B.; Spencer, P.J. *Materials Thermochemistry*, 6th ed.; Pergamon Press: Oxford, UK, 1993; pp. 254–326.
30. Wu, J.; Wei, X.Z.; Pature, N.P.; Klemens, P.G.; Gell, M.; Garcia, E.; Miranzo, P.; Osendi, M.I. Low-thermal-conductivity rare-earth zirconates for potential thermal-barrier-coating applications. *J. Am. Ceram. Soc.* **2002**, *85*, 3031–3035. [[CrossRef](#)]
31. Evans, A.G.; Charles, E.A. Fracture toughness determinations by indentation. *J. Am. Ceram. Soc.* **1976**, *59*, 371–372. [[CrossRef](#)]
32. Berman, R. *Thermal Conduction in Solids*; Clarendon Press: Oxford, UK, 1976; pp. 1–101.
33. Lehmann, H.; Pitzer, D.; Pracht, G.; Vassen, R.; Stover, D. Thermal conductivity and thermal expansion coefficients of the lanthanum rare-earth-element zirconate system. *J. Am. Ceram. Soc.* **2003**, *86*, 1338–1344. [[CrossRef](#)]
34. Wan, C.; Qu, Z.; Du, A.; Pan, W. Influence of B site substituent Ti on the structure and thermophysical properties of A₂B₂O₇-type pyrochlore Gd₂Zr₂O₇. *Acta Mater.* **2009**, *57*, 4782–4789. [[CrossRef](#)]
35. Shannon, R.D. Revised effective ionic radii and systematic studies of interatomic distances in halides and chalcogenides. *Acta Crystallogr. Sect. A* **1976**, *32*, 751–767. [[CrossRef](#)]

36. Wang, Y.; Yang, F.; Xiao, P. Role and determining factor of substitutional defects on thermal conductivity: A study of $\text{La}_2(\text{Zr}_{1-x}\text{B}_x)_2\text{O}_7$ (B = Hf, Ce, $0 \leq x \leq 0.5$) pyrochlore solid solutions. *Acta Mater.* **2014**, *68*, 106–115. [[CrossRef](#)]
37. Schulz, U. Phase transformation in EB-PVD yttria partially stabilized zirconia thermal barrier coatings during annealing. *J. Am. Ceram. Soc.* **2000**, *83*, 904–910. [[CrossRef](#)]
38. Curry, N.; VanEvery, K.; Snyder, T.; Markoscan, N. Thermal conductivity analysis and lifetime testing of suspension plasma-sprayed thermal barrier coatings. *Coatings* **2014**, *4*, 630–650. [[CrossRef](#)]
39. Zhao, M.; Ren, X.; Pan, W. Effect of lattice distortion and disordering on the mechanical properties of titania-doped yttria-stabilized zirconia. *J. Am. Ceram. Soc.* **2014**, *97*, 1566–1571. [[CrossRef](#)]
40. Mercer, C.; Williams, J.R.; Clarke, D.R.; Evans, A.G. On a ferroelastic mechanism governing the toughness of metastable tetragonal-prime (t') yttria-stabilized zirconia. *Proc. R. Soc. A* **2007**, *463*, 1393–1408. [[CrossRef](#)]
41. Evans, A.G. Perspective on the development of high-toughness ceramics. *J. Am. Ceram. Soc.* **1990**, *73*, 187–206. [[CrossRef](#)]



© 2018 by the authors. Licensee MDPI, Basel, Switzerland. This article is an open access article distributed under the terms and conditions of the Creative Commons Attribution (CC BY) license (<http://creativecommons.org/licenses/by/4.0/>).